Biointerphases
A Journal of Biomaterials and Biological Interfaces

Comparison of 20 nm silver nanoparticles synthesized with and without a gold core: Structure, dissolution in cell culture media, and biological impact on macrophages

Prabhakaran Munusamy, Chongmin Wang, Mark H. Engelhard, Donald R. Baer, Jordan N. Smith, Chongxuan Liu, Vamsi Kodali, Brian D. Thrall, Shu Chen, Alexandra E. Porter, and Mary P. Ryan

Citation: Biointerphases **10**, 031003 (2015); doi: 10.1116/1.4926547
View online: http://dx.doi.org/10.1116/1.4926547
View Table of Contents: http://scitation.aip.org/content/avs/journal/bip/10/3?ver=pdfcov
Published by the AVS: Science & Technology of Materials, Interfaces, and Processing

Comparison of 20 nm silver nanoparticles synthesized with and without a gold core: Structure, dissolution in cell culture media, and biological impact on macrophages

Prabhakaran Munusamy, Chongmin Wang, Mark H. Engelhard, and Donald R. Baer[a)]
Environmental Molecular Sciences Laboratory, Pacific Northwest National Laboratory, Box 999, Richland, Washington 99354

Jordan N. Smith, Chongxuan Liu, Vamsi Kodali, and Brian D. Thrall
Fundamental and Computational Sciences Directorate, Pacific Northwest National Laboratory, Box 999, Richland, Washington 99354

Shu Chen, Alexandra E. Porter, and Mary P. Ryan
Department of Materials and London Center for Nanotechnology, Imperial College London, Exhibition Road, SW72AZ London, United Kingdom

(Received 19 February 2015; accepted 30 June 2015; published 15 July 2015)

Widespread use of silver nanoparticles raises questions of environmental and biological impact. Many synthesis approaches are used to produce pure silver and silver-shell gold-core particles optimized for specific applications. Since both nanoparticles and silver dissolved from the particles may impact the biological response, it is important to understand the physicochemical characteristics along with the biological impact of nanoparticles produced by different processes. The authors have examined the structure, dissolution, and impact of particle exposure to macrophage cells of two 20 nm silver particles synthesized in different ways, which have different internal structures. The structures were examined by electron microscopy and dissolution measured in Rosewell Park Memorial Institute media with 10% fetal bovine serum. Cytotoxicity and oxidative stress were used to measure biological impact on RAW 264.7 macrophage cells. The particles were polycrystalline, but 20 nm particles grown on gold seed particles had smaller crystallite size with many high-energy grain boundaries and defects, and an apparent higher solubility than 20 nm pure silver particles. Greater oxidative stress and cytotoxicity were observed for 20 nm particles containing the Au core than for 20 nm pure silver particles. A simple dissolution model described the time variation of particle size and dissolved silver for particle loadings larger than 9 μg/ml for the 24-h period characteristic of many *in-vitro* studies. [http://dx.doi.org/10.1116/1.4926547]

I. INTRODUCTION

The use of Ag nanomaterials in consumer products has led to the release of nanoparticles and Ag dissolved from the particles into the environment, making it important to understand nanoparticle transformations in relevant media and the implications for environmental and human health.[1] A wide variety of synthesis techniques and routes make it possible to produce Ag nanoparticles (AgNPs) of controlled size, shape, and surface functionality optimized for specific applications.[2–13] Pure AgNPs ($Ag^{P}NPs$) grown and structured in a variety of ways[14] are used in many applications, although challenges related to uniformity and stability remain.[15] There is growing interest in AgNPs with Au cores ($Ag^{Au}NPs$) due to the ability to tune or optimize their optical and catalytic behaviors.[16,17] Both Ag and Au–Ag core–shell particles are available commercially.[18]

Nanoparticles, transformed nanoparticles, and Ag dissolved from the particles have each been associated with biological effects. Although AgNPs themselves have been observed to be toxic,[19] dissolved Ag in the form of ions, or Ag complexed with other components of the media, has been demonstrated to be toxic to bacteria,[20] biofilms,[21] aquatic organisms,[22] and algae.[23,24] The detailed nature of the particles can be important; George *et al.*,[25] as one example, suggested that surface defects in Ag nanoplatelets had a strong impact on particle toxicity. The specific media also influence particle fate.[26] Although Au and Ag/Au particles intended for cancer therapy were stable in the synthesis and storage media, they were observed to be highly unstable in biological media.[27] Cell culture models of toxicity are routinely utilized for hazard assessment, and robust understanding of cellular dosimetry to AgNPs, Ag ions, and ionic complexes is needed for proper interpretation of these studies. Therefore, knowledge of the nature of the initial particles, along with their transformations and stability in biological media, is important to understanding the biological impact of nanoparticles.

In addition to the initial nature of the particles and the dispersion media, experimental conditions, such as *p*H, $_{P}O_2$, and particle concentrations, will impact AgNP particle stability and biological response.[12,28,29] The confounding influences of these factors can make it difficult to compare dissolution data and biological impacts[30] reported in the literature as

[a)]Electronic mail: don.baer@pnnl.gov

demonstrated by the wide variation in the amounts of Ag observed to dissolve during *in-vitro* studies with a range of seemingly inconsistent biological impacts.[6,25,31–37] After testing several AgNPs, Matzke *et al.*[18] found no clear relationship between toxicity and different particle shapes, sizes, or coatings.[18] They suggest an "intricate interplay between particle characteristics and the media in which the tests are carried out." Upon transfer to test media, particles often increased in size due to agglomeration and adsorption of proteins, both of which can alter (inhibit or promote) dissolution and particle transformation.[35,38] Silver ions produced by dissolution may bind to proteins in the media or react with inorganic components in the media. Silver ions released by dissolution of Ag nanowires inside epithelial cells have been observed to form an insoluble Ag_2S precipitate.[39,40]

The measurements reported here are associated with a National Institute of Environmental Health Sciences (NIEHS) Centers for Nanotechnology Health Implications Research (NCNHIR) consortium examining the toxicology of nanoparticles. Specifically, 20 and 110 nm particles grown using 7–8 nm Au seed particles having citrate coatings were prepared by NanoComposix (San Diego, CA) for consortium use. These particles are identified as $Ag^{Au}{}_{20}$NP and $Ag^{Au}{}_{110}$NP. Another set of 20 nm particles were provided by NanoComposix without the Au seed ($Ag^{pn}{}_{20}$NP). For comparison, we also examined 20 nm silver particles with citrate coatings grown at Imperial College London ($Ag^{pi}{}_{20}$NP).

As already noted, the wide variety of synthesis methods, the addition of different particle of coatings, the dispersion in different cell culture media, and determining the responses of different cell types all complicate comparison of results from different studies. To make the comparison behaviors of two different 20 nm AgNPs possible in this study, our approach was to minimize the parameters to be varied. We characterized the particles including their structures, measured dissolution in the cell culture media being used for *in-vitro* studies at Pacific Northwest National Laboratory (PNNL) [Rosewell Park Memorial Institute (RPMI) 1640 culture medium supplemented with fetal bovine serum (FBS)][41] and assessed if differences in the particles would cause differences in biological responses of macrophage cells. Therefore, as many parameters as possible were kept constant, all particles examined had been stabilized in a citrate solution (e.g., all started with nominally the same coating), the samples were disbursed using the same process, tested in the same media, and exposed to the same cell line. The biological outcomes reported here are preliminary in that they inform more detailed and comprehensive tests of the biological response to AgNPs to be reported later.

II. MATERIALS AND METHODS

A. Ag nanomaterials sources and materials handling

Citrate-stabilized AgNPs ~20 and 110 nm in diameter were used in this study. AgNPs particles with ~7 nm Au cores (lot/batch number MGM 1659) of size 20 and 110 nm ($Ag^{Au}{}_{20}$NPs and $Ag^{Au}{}_{110}$NPs) and a batch of pure Ag particles $Ag^{pn}{}_{20}$NP were supplied by NCNHIR consortium (purchased from nanoComposix, San Diego, CA). Arrival dates of all stock solutions for each particle type are included in Table S1.[42] Pure AgNPs of primary size ~20 nm ($Ag^{pi}{}_{20}$NPs) were synthesized at the Imperial College London, using a borohydride reduction method. The first batch of Ag-NPs particles was observed to have significant agglomeration within 3 months, and a second batch was used to complete the studies. As-received particles in stock solutions in 30 ml plastic containers were stored in a refrigerator at 4 °C before any further processing for designed dissolution experiments. Stock particles from both sources were constituted in ~2 mM citrate buffer solution. These stock nanoparticle suspensions, 1 mg/ml for Ag^{Au}NPs and 0.5 mg/ml for $Ag^{pi}{}_{20}$NPs, were diluted in deionized (DI) water for particle size measurements by dynamic light scattering (DLS). For dissolution experiments, stock particle solution was dispersed in culture media according to Scheme 1.

B. Chemicals

RPMI 1640 and FBS serum were commercially purchased from Atlanta Biologicals (Flowery Branch, GA). The complete culture media was made up of a mixture of RPMI and

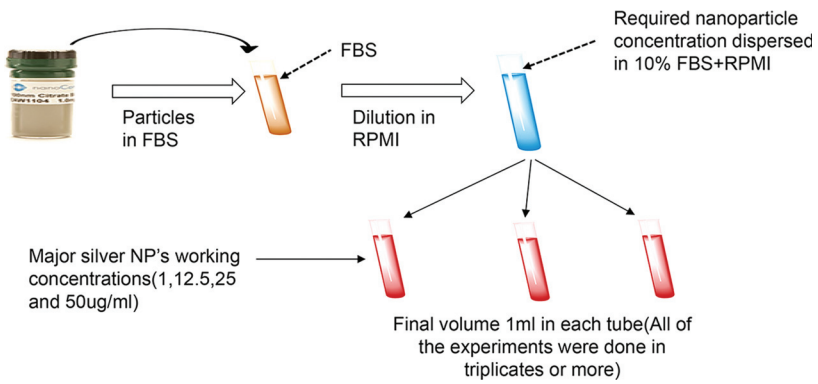

SCHEME 1. AgNP dispersion protocol followed for PNNL toxicology for *in-vitro* toxicity studies. Nanoparticles from the stock solution were directly diluted in concentrated FBS to minimize agglomeration of particles followed by the addition of RPMI 1640.

FBS (10% volume). DI water used in these studies was produced by a Millipore filter system and had 18.2 mΩ conductivity at 25 °C, with 4 ppb total organic carbon. Acid solution (70% double distilled nitric acid and double distilled concentrated hydrochloric acid) was obtained from GFS Chemicals, Inc. (Columbus, OH, USA).

C. Preparation of Ag nanoparticles suspension in culture media (FBS 10%+RPMI 1640)

We followed the process used by our biological team for the delivery of nanoparticles to cells for *in-vitro* studies (Scheme 1).[41] Nanoparticles initially suspended in citrate buffer were first dispersed in concentrated FBS solution followed by the addition of RPMI 1640 to make the total volume of FBS 10%. For dissolution experiments, Ag^{P}_{20}NPs and Ag^{Au}NPs nanoparticles were prepared at concentrations of 1–50 μg/ml. All the sample preparation was performed at room temperature.

D. DLS particle size and zeta potential measurements

Hydrodynamic particle sizes and zeta potentials were measured using a Brookhaven Instrument Corporation (Holtsville, New York) ZetaPALS® (Zeta Potential Analyzer using Phase Analysis Light Scattering) instrument. Hydrodynamic diameters of particles were calculated from intensity-weighted average translational diffusion coefficient using cumulant analysis on the autocorrelation function using vendor-provided software. Zeta potential measurements were performed using a platinum electrode immersed in the particle suspension and surface charge values derived from electrophoretic mobility of particles under the influence of an applied field. Smoluchowski's equation was applied in vendor-provided software to derive the numerical zeta value. All size measurements were performed in triplicate with more than one run for each set. Before particle size and surface charge measurements, the stock particle solutions were warmed to room temperature for a minimum of 10 min. After warming, the solutions were sonicated for ∼3 min to break up weak agglomerates and then vortexed to create a uniform particle suspension. These measurements were performed at room temperature. For kinetic studies, particle suspensions remained inside the DLS sample holder and data was collected using automated data collection.

E. X-ray diffraction measurements

Silver nanoparticles were concentrated for x-ray diffraction (XRD) measurements by centrifuging 1 ml of stock solution at 30 000 rpm for 20 min and removing the supernatant. The particles suspensions were dried on zero-background quartz substrate to leave a thin film of nanoparticles. The scans were collected using a Panalytical Bragg–Brentano diffractometer with Cu Kα radiation, automatic divergence slits, and a postdiffraction monochromator. Data were collected between 20° and 120° 2-theta and analyzed using the fundamental parameters approach using Pawley fits to the data implemented in TOPAS v4.2 (Bruker AXS). The starting cell parameters for the Pawley fits were obtained from International Centre for Diffraction Data database entries 0-04-783 (Ag) and 0-04-784 (Au).

F. Scanning and high resolution-transmission electron microscopy

Structural features of the nanoparticles were analyzed using both scanning/transmission electron microscopy (S/TEM) and high resolution TEM (HR-TEM) imaging. For S/TEM imaging, the FEI-Titan 80–300 microscope equipped with a probe-forming lens corrector was used and operated at an accelerating voltage of 300 keV. The high angle annular dark-field (HAADF) image collection angle was 50–200 mrad. HR-TEM images were captured with a FEI-Titan 80–300 microscope fitted with an image corrector. All TEM samples were prepared by drop casting a drop of suspension on a 200 mesh lacey carbon TEM grid. Nanoparticles following dissolution and transformation in cell culture medium (according to Scheme 1) were also prepared in a similar way; particles were dispersed at a concentration of 1 μg/ml and placed in an incubator at 37 °C for 24 h. These particles were prepared for imaging by placing a drop of the solution onto a TEM grid. As-received particles subjected to dissolution conditions were prepared by following the same procedure and conditions. The mean time between sample grid preparation and imaging was minimized (typically 10 min or less), and the samples were dried in the vacuum of the entry port to decrease exposure of particles to ambient atmosphere and inhibit further dissolution or transformation. Particle images shown were collected by scanning and spotting particles around different regions of the sample grid. Control tests were conducted to determine if beam damage caused or enhanced any of the results reported.

G. Quantitative dissolution measurements by inductively coupled plasma-mass spectrometry

Time-dependent dissolution of AgNPs was measured in cell culture media at varying nanoparticle concentrations following Scheme 2. Suspensions of AgNPs (1 ml) were prepared in triplicate by mixing Ag nanoparticle stock into FBS, followed by the addition of RPMI (Scheme 1). Final concentrations of nanoparticle suspensions ranged from 1 to 50 μg/ml in RPMI with 10% FBS. Nanoparticle suspensions were maintained in a cell culture incubator at standard conditions (37 C, ∼5% CO_2), and at selected times consistent with *in-vitro* studies (e.g., 0, 2, 6, or 24 h), nanoparticle suspensions were removed and ultracentrifuged at 30 000 rpm (49 000 × g maximum, 38 000 × g average, and 27 000 × g minimum) for 90 min. After centrifugation, aliquots of supernatants (∼200 μl) were collected, and silver levels were quantified using inductively coupled plasma-mass spectrometry (ICP-MS).

Samples for ICP-MS were digested with ∼0.5 or 2 ml of 70% double-distilled nitric acid for ∼2 h or overnight until clear, and then ∼0.5 or 1 ml of double distilled concentrated hydrochloric acid was added to shift the equilibrium from

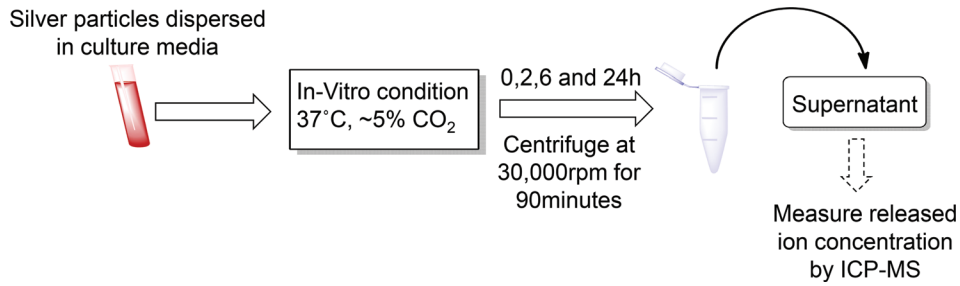

SCHEME 2. Steps and conditions followed for nanoparticles dissolution experiments. Additional details provided in the text.

insoluble to soluble silver chloride complexes. Aliquots were diluted to 2% nitric acid and total silver was quantified using an Agilent 7500 CE (Santa Clara, CA, USA) inductively coupled plasma-mass spectrometer. ^{107}Ag was quantified in helium collision mode using ^{45}Sc and ^{115}In (10 ng/ml) as internal standards. Additionally, ^{109}Ag was also monitored. Three rinses with 2% nitric acid between runs were used to minimize carryover. Quantification was accomplished using a linear model fit to calibration curves (VHG Labs, Inc., Manchester, NH, USA) created by spiking Ag into 2% nitric acid or into RPMI+10%FBS mixture. Measurements on the RPMI/FBS mixture contained Y as an internal standard. Limits of quantitation for silver were ~0.1 ng/ml for samples diluted in 2% nitric acid.

H. HMOX1 western blot

RAW 264.7 macrophage cells were exposed to AgNPs at various concentrations for 24 h and examined for oxidative response and cytotoxicity. For the oxidative response tests, the cells were lysed using phosphate-buffered saline (PBS) buffer with 2% NP-40 containing protease cocktail inhibitor (Roche, Inc., Cat#11836153001). The lysed proteins were diluted in equal concentration in lithium-dodecyl-sulfate buffer and separated electrophoretically under reducing conditions on a 4%–12% bis–tris polyacrylamide gel in 2-(N-morpholino)ethanesulfonic acid) sodium dodecyl sulfate running buffer (Invitrogen, Carlsbad, CA). The electrophoretically separated proteins were transferred to a polyvinylidene difluoride membrane (Invitrogen, Carlsbad, CA). Membranes were blocked for 1 h at room temperature in a 5% w/v solution containing nonfat milk in PBS. Western blot analysis was used to measure the level of induction of heme oxygenase (HMOX1), a common antioxidant response protein that is regulated by redox-sensitive transcription factors. HMOX1 was detected on the blot using Anti-Heme Oxygenase 1 (Abcam, Inc., Cat# ab52947) for 12 h at 40 C in PBS containing 1% w/v milk and antibody at (1:1000 dilution) followed by incubation for 1 h at room temperature with Goat antirabbit horseradish peroxidase secondary antibody (Jackson Immuno Research, Inc., Cat# 111-035-003) at 1:2000 dilution in PBS containing 1% w/v milk. The membranes were washed in PBS with 1% Tween 20 prior to development with SuperSignal West Pico ECL (enhanced chemiluminescent substrate) (Thermo Scientific, Rockford, IL) according to the manufacturer's instructions. HMOX1 Band intensities were quantified using NIH IMAGEJ (http://imagej.nih.gov/ij/).

I. Cytotoxicity

The cytotoxicity of AgNPs was evaluated using propidium iodide (PI)/Hoechst 33342 (Hoechst). Cells were plated at 4.17 × 104 cells/cm^2 in a 24 well plate. After cells were plated overnight, cells were exposed to the AgNPs at the required concentration for 24 h. To determine the cytotoxicity, cells were incubated at 37 °C with 1.5 mM PI (Sigma, Cat# P-4170) and 16.7 μM Hoechst (Anaspec, Inc., Cat#83218) for 15 min. After incubation, the cells were washed once with PBS. The media, staining solution, and washes were collected, spun down, and the cell pellet was resuspended in 1:1 mix of Trypan blue (Sigma, Cat#T8154) and PBS. The live/dead cells in the supernatants were quantified using a hematocytometer. The live/dead cells on the plates were quantified using Nikon Eclipse TE300. The live/dead cells from the images were quantified using NIH IMAGEJ. The final cytotoxicity = 100 × (total dead cells/total cells), where total was the sum of cell counts from supernatants and cells on the plate.

J. XPS and optical absorption

To determine the presence of impurities and examine the presence of surface coatings x-ray photoelectron spectroscopy (XPS) measurements on nanoparticles were made using a PHI Quantera. Drops of suspensions containing AgNPs were deposited on a Si wafer substrates and dried before analysis. Optical absorption measurements were made on particle suspended in various media using a Varian Cary-1 UV-visible (UV-vis) spectrophotometer.

III. RESULTS

A. Characterization of as-received AgNPs

1. Particle size, surface charge, and surface composition

The effective hydrodynamic diameters, d_{eff}, determined by DLS and the zeta potentials of the as-received particles are shown in Table I. Measurements for Ag^{Au}NPs had been conducted in a NaCl solution at the National Characterization Laboratory (NCL) of National Cancer

TABLE I. Hydrodynamic particle size and surface charge measured for Ag and Ag-gold particles in DI water and culture media.

Designation	Nanomaterial	Z-average diameter DLS (nm) in 2 mM NaCl	Effective diameter d_{eff} (nm) in DI water		Polydispersity index (PDI)		Zeta potential (mV) In 10 mM NaCl	Zeta potential (mV) In DI water	Effective diameter d_{eff} (nm)
		NCL	PNNL		NCL	PNNL	NCL	PNNL	In 10%FBS+RPMI
$Ag^{Au}{}_{20}$NPs	20 nm Ag-gold citrate	24 ± 0.1	29 ± 0.7		0.06	0.124	−48 ± 5	−31 ± 7	52 ± 8
$Ag^{Au}{}_{110}$NPs	110 nm Ag-gold citrate	104 ± 0.4	110 ± 0.7		0.084	0.106	−43 ± 3.6	−40 ± 2	136 ± 1.8
$Ag^{pi}{}_{20}$NPs	20 nm Ag citrate	—	29 ± 1		—	0.364	—	−29 ± 1.3	41 ± 0.95
$Ag^{pn}{}_{20}$NPs	20 nm Ag citrate	—	29.5 ± .5		—	0.18	—	−38 ± 1	57 ± 0.7

Institute Laboratory before distribution to consortium members. Hydrodynamic particle sizes (d_{eff}) measured at PNNL in DI water were generally consistent with those determined at NCL. Two batches of $Ag^{pi}{}_{20}$NPs and the $Ag^{pn}{}_{20}$NPs had similar hydrodynamic sizes ≈29 nm. Size distributions for all particles are shown in Fig. S1 and Table S2.[42] The $Ag^{Au}{}_{20}$NPs, $Ag^{Au}{}_{110}$NPs, and $Ag^{pn}{}_{20}$NPs were monomodal in size distribution with polydispersity indices (PDIs) less than 0.2. The $Ag^{pi}{}_{20}$NPs were monomodal with a somewhat wider size distribution as indicated by higher polydispersity value. The hydrodynamic size as measured by DLS was typically larger than the physical size of the particles as determined by methods such as TEM. The shape, size, and morphology of the particles are discussed in more detail below.

All of the AgNPs were negatively surface charged in 10 mM NaCl and DI water, consistent with the citrate coating used for stabilization of particles against agglomeration. Although there were minor differences in size and PDIs of the two batches of $Ag^{pi}{}_{20}$NPs, their dissolution and other behaviors were virtually identical so no distinction was made when reporting them. All particles were examined using XPS to verify the surface and bulk compositions were as expected (Figs. S2–S5). The elements present and the chemical state of the carbon photoelectron peaks were consistent with citrate coated AgNPs along with the presence of some adventurous carbon. As reported earlier, the Au cores for $Ag^{Au}{}_{20}$NPs appeared in XPS measurements and the data provided supplementary material[42] about the Ag-shell Ag-core shell nature of the particles.[43] The Au cores were not visible by XPS for the $Ag^{Au}{}_{110}$NPs.

After transfer to the culture medium, the hydrodynamic diameter of particles increased (Table I). UV-vis spectroscopy analysis on particles coated with proteins in DI water or PBS showed slight red shift consistent to the particle size increase (Fig. S6). No other peaks at longer wavelength could be observed in DI water or PBS in the presence of FBS, indicating the presence of particles as individual particles. This increase in size (representing coating thicknesses averaging approximately 10 nm) was consistent with literature reported FBS protein coating thicknesses, which range from 10 to 25 nm.[44,45] Particles dispersed in the cell culture media at room temperature remained in solution and maintained a stable size (as listed in Table I) for longer than 24 h although UV-vis spectra particles in RPMI-FBS mixture had a secondary peak, indicating that some agglomeration had also occurred (Fig. S6).

2. Morphology and structure

The morphology and structure of as-received particles were examined by electron microscopy and XRD. HAADF STEM and HR-TEM images of the $Ag^{Au}{}_{20}$NPs, $Ag^{pi}{}_{20}$NPs, and $Ag^{pn}{}_{20}$NPs were conducted to examine the size, morphology, and grain structure of the particles. Representative images are shown in Fig. 1 with additional images included in Figs. S7 and S8. As expected, the physical sizes observed

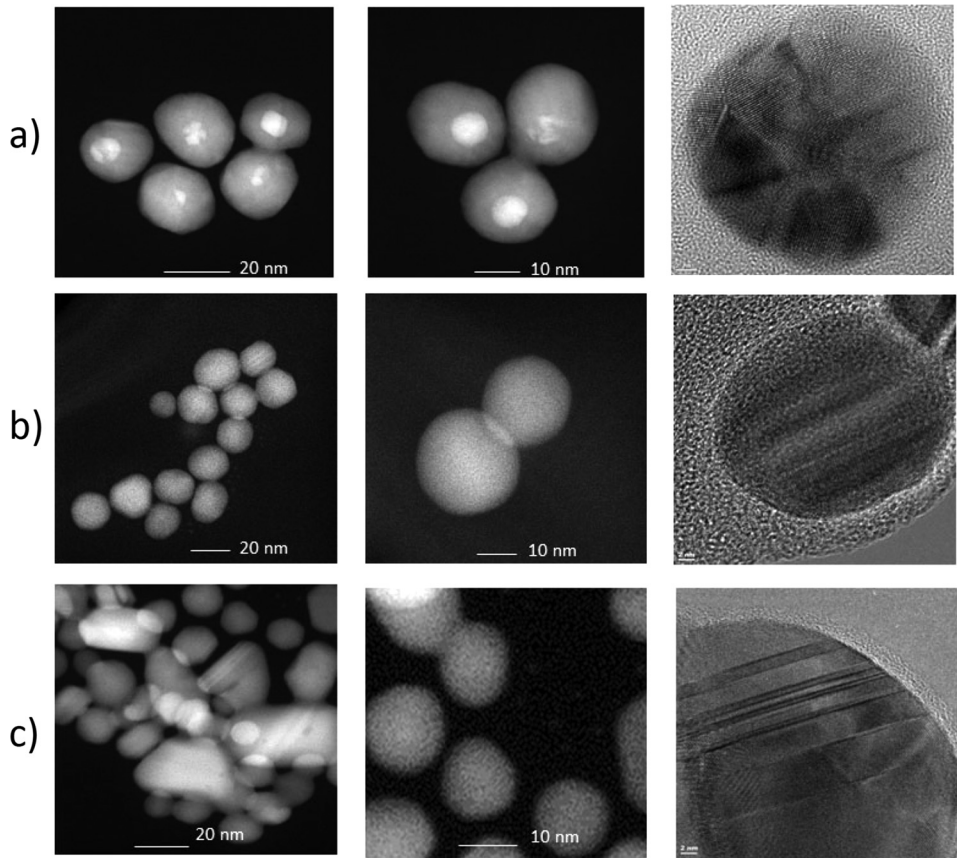

FIG. 1. Representative HAADF STEM (columns 1 and 2) and HR-TEM (column 3) images of the (a) $Ag^{Au}{}_{20}$NPs, (b) $Ag^{pn}{}_{20}$NPs, and (c) $Ag^{pi}{}_{20}$NPs stock particles.

by TEM were nominally 20 nm diameters, smaller than the hydrodynamic sizes measured by DLS. The $Ag^{pi}{}_{20}$NPs [Fig. 1(c)] showed the largest variation in particle size and shape consistent with a larger PDI value in Table I. The $Ag^{pn}{}_{20}$NPs shown in Fig. 1(b) are not as uniform in size as the $Ag^{Au}{}_{20}$NPs as also indicated by a slightly higher PDI.

The HAADF-STEM images highlight the Au cores of $Ag^{Au}{}_{20}$NPs [Fig. 1(a)]. Intensities observed in HAADF-STEM images vary as Z^2 of the scattering atoms. Therefore, the core Au particle with higher atomic number (79) appeared significantly brighter than the silver shell (atomic number of 47). These images were consistent with the ~7–8 nm Au particles used as seeds to grow particles of uniform size.[46,47] The gold core did not always appear to be centered within the particles, and some of the gold seeded particles were significantly distorted from a spherical shape. The interface partition between the Ag and Au layer in $Ag^{Au}{}_{20}$NPs appeared to be sharp, supporting the core–shell structure rather than an alloy formation.

The $Ag^{Au}{}_{110}$NPs, which were also seeded using ~7 nm Au seeds, appeared to be quasispherical with uniform size distribution (see Fig. S8). Due to the small percent of Au in these larger particles, Au cores in these particles were only visible in a higher magnification image. Although the presence of the Au core was visible in the HAADF-STEM images, the crystallite structure (but not the gold core) was more apparent in HR-TEM, as shown in Fig. 1. Because the crystal structure (face centered cubic) and lattice constants of Ag (0.408 nm) and Au (0.407 nm)[48,49] are nearly identical, the Au cores were not visible in the phase contrast HR-TEM images.

3. Structure of particles

The images shown in Fig. 1 provide structural information about the three types of 20 nm AgNPs. The structure of $Ag^{pn}{}_{20}$NPs and $Ag^{pi}{}_{20}$NPs was significantly different to that of the $Ag^{Au}{}_{20}$NPs. Both sets of pure AgNPs exhibited a relatively uniform structure with a few visible planar defects (stacking faults or grain boundaries) aligned along particular crystallographic directions [Figs. 1(b) and 1(c)]. In contrast, $Ag^{Au}{}_{20}$NPs are composed of many highly disordered domains characteristic of multiple twined particles. The difference in structure of particles is likely due to difference in synthesis route and the presence of the Au core. The origin of separate domains was likely due to heterogeneous nucleation growth mechanism as described previously for many seeded nanostructures growth including Au–Ag core–shell nanocrystals.[14,50] The $Ag^{pi}{}_{20}$NPs synthesized by a homogenous nucleation process (via borohydride reduction, Scheme S1) were structurally more uniform showing slip planes and made up of relatively few grains.

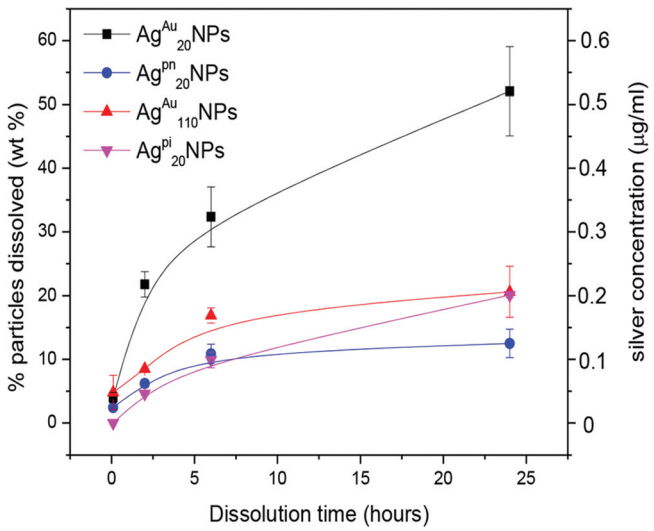

FIG. 2. Dissolution profile showing amount of Ag in the supernatant and percent of particles dissolved for $Ag^{Au}{}_{20}$NPs, $Ag^{pn}{}_{20}$NPs, $Ag^{Au}{}_{110}$NPs, and $Ag^{pi}{}_{20}$NPs in FBS 10% volume + RPMI culture media.

Fitting the XRD data (Fig. S9) using the Debye–Scherrer equation provides an estimate of grain sizes within the particles, which supports the TEM observations. The $Ag^{Au}{}_{20}$NPs were made up of many ~7 nm Ag grains nucleated around the Au core, while the two pure 20 nm AgNPs had larger grain sizes ($Ag^{pi}{}_{20}$NPs ~ 15 nm and $Ag^{pn}{}_{20}$NPs ~ 13 nm), somewhat smaller than the average particle sizes. The $Ag^{Au}{}_{110}$ NPs were composed of ~55 nm grains of Ag as indicated by XRD and consistent with HR-TEM measurements (Fig. S3). In summary, the $Ag^{P}{}_{20}$NPs had a relatively ordered structure in comparison to the disordered and potentially higher energy structures of the $Ag^{Au}{}_{20}$NPs. The $Ag^{Au}{}_{110}$NPs were made up of grains with sizes significantly larger than those in the $Ag^{Au}{}_{20}$NPs.

B. Dissolution and transformation

1. Comparison of dissolution of four AgNPs in cell culture media

The release of silver from the four types of AgNPs was measured in cell culture media using conditions and methods used for Scheme 2. For the initial comparison, each type of nanoparticle was dispersed in medium at a concentration of 1 μg/ml. The weight percentage of particles dissolved and Ag concentration measured in solution as a function of time are shown in Fig. 2. The initial increase of dissolved Ag was rapid and the rate of increase decreased at longer times, as expected in the closed system as the driving force for dissolution decreased with the increasing amount of dissolved Ag. During the 24-h period, a higher amount of Ag was released from $Ag^{Au}{}_{20}$NPs into the supernatant (0.5 μg/ml and 50% of particle mass) in comparison to other particles. For the same time period, the $Ag^{pi}{}_{20}$NPs, $Ag^{pn}{}_{20}$NPs, and $Ag^{Au}{}_{110}$NPs dissolved 20% (0.2 μg/ml) or less of the total initial particle mass. As the total surface area of the 110 nm particles was less than the 20 nm particles at the same mass loading, the initial rate of dissolution for the larger particles was expected to be slower, as observed. In this case, AgNPs of similar size, synthesized by different chemical routes with different microstructures, dissolved at different rates and released significantly different amounts of Ag into the supernatant during the 24-h period.

The evolution of morphology of $Ag^{Au}{}_{20}$NPs and $Ag^{P}{}_{20}$NPs during dissolution was examined by HAADF-STEM after 24 h in cell culture media. These specimens were prepared following Scheme 1, but were formed by dropping solution onto TEM grids without centrifugation or other processing of Scheme 2. Figure 3 shows images of $Ag^{Au}{}_{20}$NPs and $Ag^{pn}{}_{20}$NPs before [Figs. 3(a) and 3(d)] and after 24 h incubation in cell culture media [Figs. 3(b), 3(c), 3(e), and 3(f)]. Consistent with the dissolution measurements, the $Ag^{Au}{}_{20}$NPs changed significantly in size and

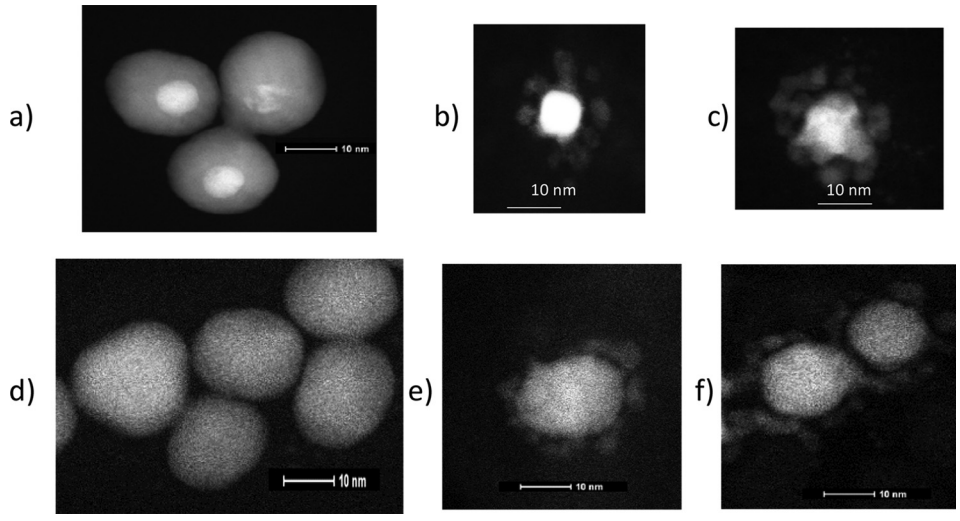

FIG. 3. HAADF STEM images of $Ag^{Au}{}_{20}$NPs and $Ag^{pn}{}_{20}$NPs before and after dissolution imaged as dispersed in cell culture media after 24 h. (a) $Ag^{Au}{}_{20}$NPs before and [(b) and (c)] after dissolution. Similarly for the $Ag^{pn}{}_{20}$NPs before (d) and [(e) and (f)] after dissolution.

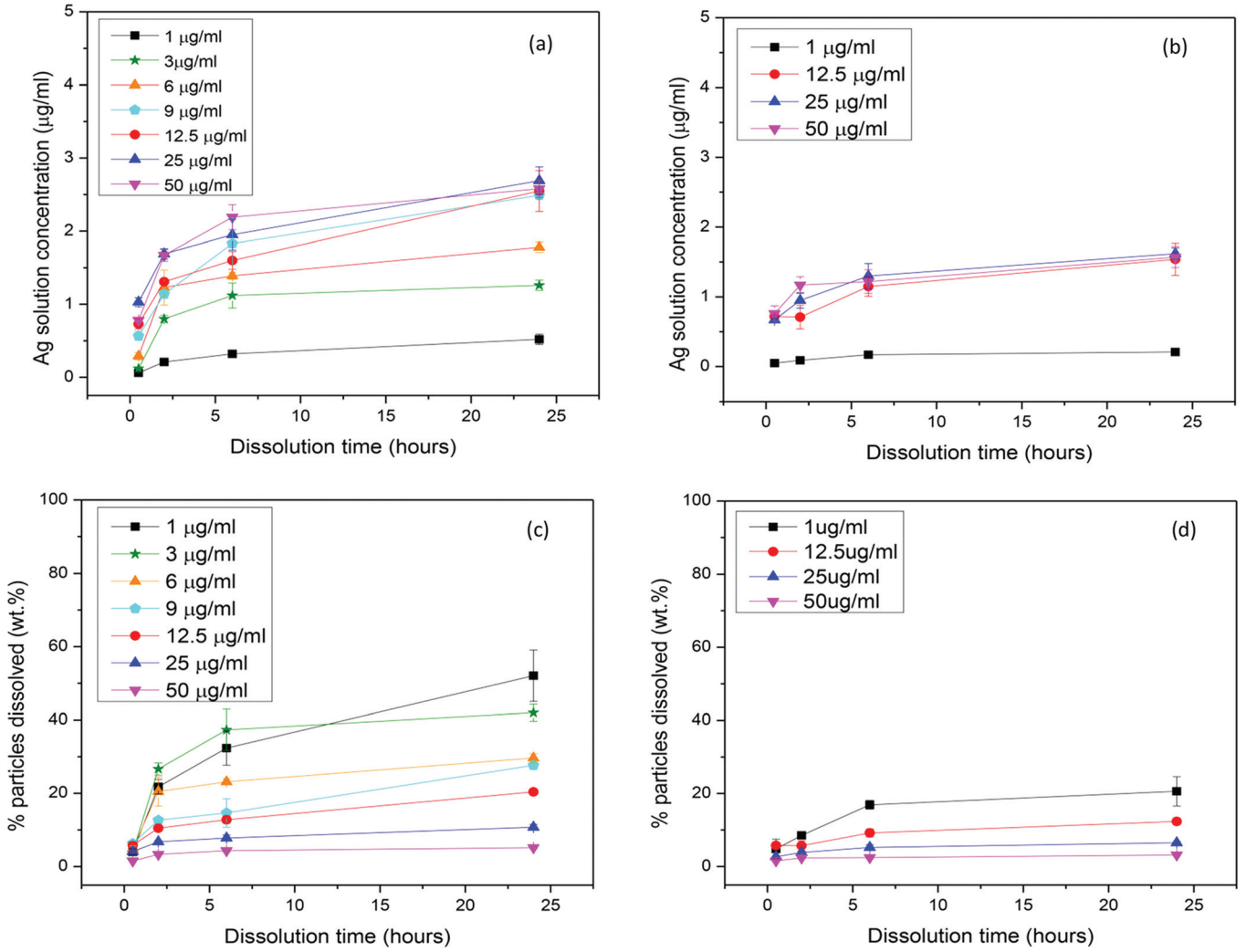

FIG. 4. Dissolution time plots for $Ag^{Au}{}_{20}$NPs [(a) and (c)], $Ag^{pi}{}_{20}$NPs [(b) and (d)] in FBS 10% volume + RPMI measured up to 24 h duration. [(a) and (b)] Plots showing ion concentration and [(c) and (d)] displaying data in terms of the percentage of the particles dissolved.

morphology after 24 h. The Au cores remained intact while significant change in the Ag shell layer occurred. The Ag shell became nonuniform in both thickness and surface morphology around the perimeter of the Au seed [Figs. 3(b) and 3(c)]. It is known that metal and metal oxide nanoparticles can undergo preferential dissolution, which is initiated at edges, corners, or defects.[51,52] The $Ag^{Au}{}_{20}$NPs underwent extensive and highly nonuniform dissolution, leaving a highly disordered structure reminiscent of the Ag shell before incubation in the cell culture medium. Secondary or Ag daughter particles (or possibly fragments of the dissolved shell for the $Ag^{Au}{}_{20}$NPs) were observed at this particle loading, but not at particle concentrations above 10 μg/ml. Some daughter particles seemed to be attached to the remnant nanoparticles (and may be residue of the initial shell) while others were located some distance away from the parent particles.

Although degradation of silver shells on the $Ag^{Au}{}_{20}$NPs was obvious from the images, $Ag^{pn}{}_{20}$ NPs were subject to less and apparently more uniform dissolution [Figs. 3(e) and 3(f)] although secondary particles were found near the primary particles, which had not changed significantly in size (consistent with less overall dissolution). Images of $Ag^{Au}{}_{110}$NPs after dissolution, shown in Fig. S10, also indicate little change in shape due to dissolution. Precipitation of pure Ag and Ag_2S nanoparticles has been observed by other researchers in a variety of experimental conditions as the product of a precipitation process.[32,53]

2. Impact of particle mass concentration on dissolution

Because *in-vitro* studies are often conducted at a variety of particle concentrations, information about dissolved Ag dose and dose rates[54] was collected at particle concentrations from 1 to 50 μg/ml. Data from a variety of particle concentrations are shown in Fig. 4 for $Ag^{Au}{}_{20}$NPs and $Ag^{pi}{}_{20}$NPs. The concentration of Ag in the supernatant is shown in the top row [Figs. 4(a) and 4(b)]. In the data of Fig. 4, dissolved

silver concentrations increased over time, providing information about the rate of dissolution.

The first time-point in the data plots was set at 0.5 h rather than 0 h. Although these measurements were for particles processed immediately after preparation without being subjected to actual *in-vitro* dissolution conditions, the particles were in the media for roughly 2 h at room temperature as Schemes 1 and 2 were being completed (with zero time at 37 °C in Scheme 2). Based on the type of particle and initial particle concentration, dissolved Ag concentrations measured at this first time increment varied between 0.05 and 1 μg/ml. The time for the first data point was selected to appear at 0.5 h in recognition that some dissolution of the AgNPs in culture medium occurred during sample processing at room temperature. Although the contribution of dissolution *during processing* did not dominate the results (the Ag concentration increases with time in solution), it is relevant to remember that particle dissolution continues at some level during sample processing before and during supernatant analysis.

Within each type of particle [Figs. 4(a) and 4(b)], but most obvious for the $Ag^{pi}{}_{20}$NPs [Fig. 4(b)], Ag concentrations in the supernatant tended to approach approximately the same levels after 24 h for particle loadings above 10 μg/ml. For the $Ag^{Au}{}_{20}$NPs after 24 h, Ag concentrations in the supernatant reached ~2.5 μg/ml while the highest Ag solution concentrations for the $Ag^{Au}{}_{110}$ NPs and $Ag^{pi}{}_{20}$NPs remained below roughly ~1.5 μg/ml. Thus, $Ag^{Au}{}_{20}$NPs were dissolved to a greater extent than other particles and produced a higher concentration of dissolved Ag in solution. The data plotted as Ag in the supernatant can be replotted as the percent of the total Ag found in the supernatant (indicating the amount of the particle dissolved) in the lower set of frames [Figs. 4(c) and 4(d)]. A simple dissolution model was applied to this form of the data (Fig. 5).

Due to the buildup of Ag concentration in solution, the initial rate of dissolution was followed by a slower increase in dissolved Ag. Therefore, much of the dissolution (up to 80%) occurred during the initial 6-h period independent of particle type or initial particle concentration as reported in other studies.[8] There appeared to be a critical particle concentration of ~9 μg/ml for the $Ag^{Au}{}_{20}$NPs, above which dissolution becomes a "saturable" process. At particle concentration of <9 μg/ml, dissolved Ag concentration after 24 h was dependent on the initial particle concentration. However, at particle concentrations of >9 μg/ml, the amount of dissolved silver concentrations in the supernatant reached a steady-state condition. However, this saturation concentration at 24 h was only apparent as longer time data (not shown) indicated that particles continued to dissolve, but at a significantly slower rate.

3. Dissolution model

The time and concentration-dependent dissolution data collected for Ag^{pi} and Ag^{Au}NPs (Fig. 4) help provide quantitative information about the nature of the particles and amount of solubilized Ag that cells would see during *in-vitro*

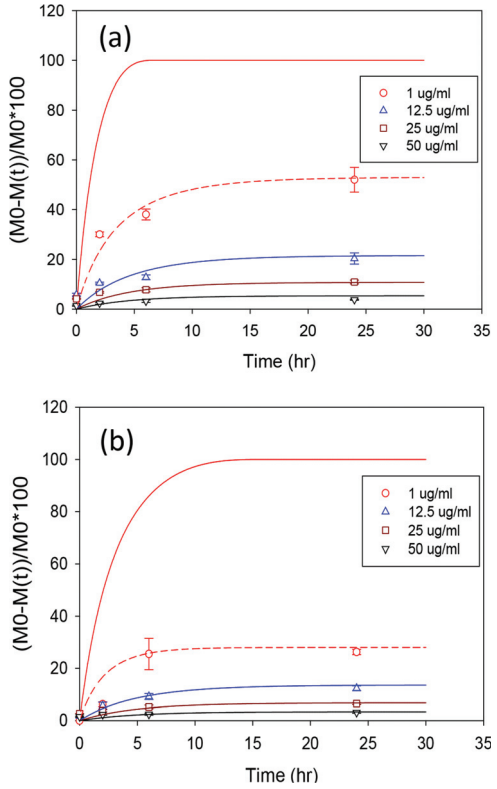

FIG. 5. Experimental data and dissolution model fit to the dissolution data as a function of time for (a) $Ag^{Au}{}_{20}$NPs and (b) $Ag^{pi}{}_{20}$NPs. The vertical axis is plotted as $[(M(0) - M(t))/M(0)] \times 100$ following Eq. (3). For each particle, the solid lines represent a single set of k_+ and K_{sp} values for that particle. Above solution concentrations of 9 μg/ml, the dissolution data can be approximately fit by single particle specific values. However, these values over predict dissolution that was observed for the lower concentrations of particles in solution, and the dashed lines are from fits to the 1 μg/ml data sets for each particle, with the values shown in Table II.

experiments at different particle loadings. The data in Fig. 4 clearly show the extent of particle dissolution and the Ag concentration in solution will vary with the type of particle, the size of the particles, and the density or loading of the particles in solution. We used a simple extension of the classical dissolution model to parameterize dissolution behaviors in solution and to extract quantitative information for comparing the qualitative observations about differences in particle behaviors.

In classical dissolution models, the overall rate of dissolution is moderated by the Gibbs free energy associated with the dissolution.[55]

$$r_{dis} = k_+ \left\{ 1 - \exp\left(\frac{G}{RT}\right) \right\}, \quad (1)$$

where r_{dis} is the overall dissolution rate, k_+ is the forward rate of dissolution, R is the gas constant, and ΔG is the Gibbs free energy change upon dissolution. The Gibbs free energy change associated with dissolution will change as products build up in solution. This formula can be somewhat simplified identifying the ratio of the activity of the reactant to species during dissolution raised to the power of their

TABLE II. Parameters obtained from fitting the experimental data to the simple dissolution model Eq. (3).

Particle concentration (μg/ml)	$Ag^{Au}{}_{20}$NPs		$Ag^{pi}{}_{20}$NPs		$Ag^{pn}{}_{20}$NPs		$Ag^{Au}{}_{110}$NPs	
	k (μg/nm^2 h)	Ksp (μg/ml)	k (μg/nm^2 h)	Ksp (μg/ml)	k (μg/nm^2 h)	Ksp (μg/ml)	k (μg/nm^2 h)	Ksp (μg/ml)
1	0.5×10^{-14}	0.53	0.4×10^{-14}	0.28	0.2×10^{-14}	0.13	0.15×10^{-14}	0.26
3	1.8×10^{-14}	1.3						
6	1.8×10^{-14}	1.8						
9	1.8×10^{-14}	2.7						
12.5	1.8×10^{-14}	2.7	1.1×10^{-14}	1.7	1.2×10^{-14}	1.0	1.6×10^{-14}	1.4
25	1.8×10^{-14}	2.7	1.1×10^{-14}	1.7			1.6×10^{-14}	1.4
50	1.8×10^{-14}	2.7	1.1×10^{-14}	1.7			1.6×10^{-14}	1.4

stoichiometric coefficients in the solution as Q and noting the equilibrium value of Q is the solubility product K_{sp}. Because $\Delta G/RT = \ln(Q/K_{sp})$[55] Eq. (1) can be rewritten as

$$r_{dis} = k_+\{1 - Q/K_{sp}\}. \quad (2)$$

At equilibrium $Q/K_{sp} = 1$ and the deviation from 1.0 gives a measure of the driving force for growth or dissolution.

This classical model can be extended to a spherical particle dissolution model to provide a framework for understanding dissolution as a function of particle concentration. Although it will be a significant oversimplification for complex biological media, dissolution in aqueous media are often understood in terms of a rate of dissolution, represented by the dissolution coefficient k, and an apparent solution solubility product, K_{sp}. These can be combined into a time-dependent dissolution model that considers the density of particles in solution and assumes that particles are spherical in shape and dissolve uniformly.

$$\frac{dC_{dissolved}}{dt} = k_+ A_o \left(\frac{M(t)}{M(o)}\right)^{\frac{2}{3}} \left(1 - \frac{C_{dissolved}}{K_{sp}}\right), \quad (3)$$

where $C_{dissolved}$ is the concentration of dissolved Ag in supernatant (μg/ml), M(t) is the mass of the particles in solution as function of time (μg or μg/ml), A_o is the initial specific surface area of particles per solution volume (nm^2/ml), k_+ is the forward rate of dissolution [from Eq. (1)], (μg/nm^2 h), and K_{sp} is the effective solubility product (μg/ml).

All time-dependent experimental data were fitted to Eq. (3). Measurements and fits to the measurements for the $Ag^{pi}{}_{20}$NPs and $Ag^{Au}{}_{20}$NPs are shown in Fig. 5 at solution concentrations of 1, 12.5, 25, and 50 μg/ml. The model fit is plotted in terms of percent of particles dissolved over time based on the initial concentration of particles in solution. The fit values of the solubility product (K_{sp}) and rate constant (k_+) are given in Table II for all measured particle concentrations and particle types. For the solution concentrations of 12.5, 25, and 50 μg/ml, the data for $Ag^{pi}{}_{20}$NPs, $Ag^{Au}{}_{20}$NPs, and $Ag^{Au}{}_{110}$NPs fit well with self-consistent single values of k_+ and K_{sp} within each particle type (e.g., single values of K_{sp} and k_+ determined for each particle fit a fairly wide range of data for the particle). Based on additional data for solution concentrations between 1 and 12.5 μg/ml for the $Ag^{Au}{}_{20}$NPs, we found single K_{sp} and k_+ values could reasonably fit the data for this particle for solution concentrations above 9 μg/ml, but significant deviations from these parameters were required to fit the data at lower concentrations. The apparent K_{sp} values for the different particles support earlier observations that $Ag^{Au}{}_{20}$NPs particles have a greater apparent solubility than $Ag^{p}{}_{20}$NPs. The results also indicate that $Ag^{Au}{}_{110}$NPs have solubility generally similar to $Ag^{p}{}_{20}$NPs. Although less extensive than for the other particles, the K_{sp} and k_+ parameters for the $Ag^{pn}{}_{20}$NPs indicate a lower apparently solubility than the $Ag^{pi}{}_{20}$NPs.

C. Biological response cellular effects of $Ag^{Au}{}_{20}$NPs and $Ag^{pn}{}_{20}$NPs

We examined if the structural and stability differences in AgNPs synthesized with or without the gold seeds were also associated with differences in biological activity (Fig. 6). Given the important role of macrophages as a first line of defense against foreign particulates, these experiments utilized the RAW 264.7 cell line as a model macrophage cell type that is commonly used for hazard assessment and mechanistic studies in nanotoxicology.[56,57] Dose-response analysis of the cytotoxic effects of AgNPs following 24-h exposure demonstrated that neither $Ag^{pn}{}_{20}$NP nor $Ag^{Au}{}_{20}$NP caused overt cytotoxicity at concentrations up to 25 μg/ml. However, a significant increase in cytotoxicity was observed at 50 μg/ml for both particle types, and this effect was exacerbated in particles containing a gold core.

The results clearly indicate that the presence of a gold core enhances the cytotoxic effects of AgNPs at high cell dose levels. However, because of the observed dissolution kinetics, there are only minor differences in the dissolved Ag to which the cells are exposed for loading at 12.5 μg/ml or higher so that the level of extracellular Ag species resulting from dissolution appears to play a relatively minor role in the dose-dependent cytotoxicity of the particles. Rather, the observed differences in the cytotoxicity of $Ag^{pn}{}_{20}$NP and $Ag^{Au}{}_{20}$NP reflect differences in interactions of the particles with the cells due to the different particles structures or the rate of dissolution and/or reactivity following intracellular uptake.

Given the induction of oxidative stress is a principal mechanism of toxicity for AgNPs, potentially through interactions between Ag ionic species and protein sulfhydryls, we

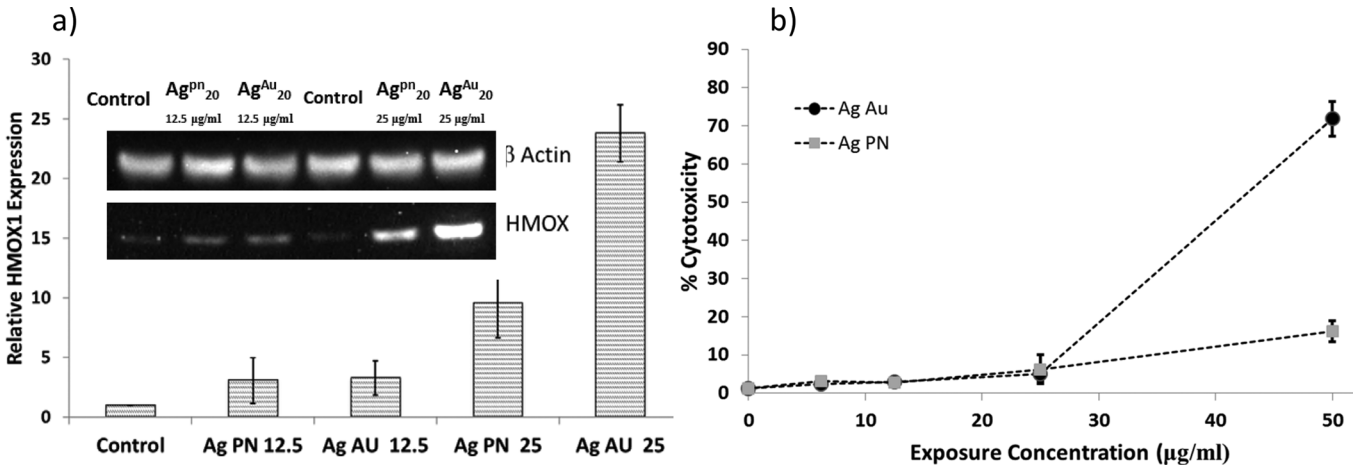

FIG. 6. (a) Exposure to Ag^{Au}_{20}NPs (core) and Ag^{PN}_{20}NPs (pure) caused differential expression of HMOX, a marker for oxidative stress in RAW 264.7 cells. The insert shows HMOX expression blot with β actin as loading control. The graph is the average HMOX expression from two independent experiments, the error bars are range of the two experimental values. (b) Exposure to Ag^{Au}_{20}NPs (circle) and Ag^{PN}_{20}NPs (square) also showed differential cytotoxicity at high nanoparticle concentrations. In both tests, the Au core particles have a greater impact at relatively high particle exposures.

also compared the relative potencies of Ag^{pn}_{20}NP and Ag^{Au}_{20}NP to induce an oxidative stress response in macrophages at subcytotoxic exposure levels. Western blot analysis was used to measure the level of induction of HMOX1, a common antioxidant response protein that is regulated by redox-sensitive transcription factors.

The results demonstrate that both AgNP types induce oxidative stress in macrophages at doses that precede overt cytotoxicity, and this response is enhanced by up to three-fold for Ag^{Au}_{20}NP compared to the same dose of particles lacking a gold core. The results are consistent with the notion that differences in intracellular dissolution and/or reactivity of the AgNPs associated with the structural alterations of the particles arising from the presence or absence of a gold core may underlie the variability in biological potency of these nanoparticles.

IV. DISCUSSION

The combination of structural, dissolution, and biological data shows that differences in AgNP synthesis route can alter particle structure and impact particle stability and biological response. Each of these is discussed individually before a more general discussion below. The combination of multiple types of data enables impacts of different parameters to be assessed.

A. Variations in particle structure and synthesis route

The Ag NPs synthesized using gold nanoparticles as seeds have a significantly different structure than nanoparticles composed of pure silver. As indicated in Fig. 1, there was less overall crystalline order in these smaller Au seeded particles in comparison to the other three types of AgNPs. The high density of crystallite boundaries and apparent disorder in Ag^{Au}_{20}NPs suggests the presence of many types of defects in Ag particles, which have been identified as highly correlated with toxicity.[25] Disorder has also been linked with increased dissolution as observed and discussed below. The grain size determined by XRD of ~7 nm for Ag^{Au}_{20}NPs was roughly consistent with the shell thickness, as expected. For the larger particles, which were also grown around an Au core, the crystallite size was much larger (~50 nm) and the defect density was expected to be lower.

B. Dissolution and transformation

1. Influence of particle structure and history on dissolution

The extent and rate of particle dissolution can be influenced by many factors including those associated with particles such as structure, degree of aggregation, surface area, shape, size, and density of defects and kink sites, and those associated with the solutions such as composition, *p*H, and chemical saturation.[58] Results of our research reinforce the role of synthesis route, particle structure and defects on particle transformation, dissolution, and solubility on the time frame of biological studies. Due to the toxicity of Ag dissolved in solution,[19] differences in solubility may impact some biological endpoints.

The microstructure differences between Ag^{Au}_{20}NPs relative to both versions of Ag^{p}_{20}NPs appear to offer an adequate explanation for much of the difference in the observed solubility. Highly disordered and amorphous structures have a higher energy state than crystalline materials, and thus, there is a free energy difference $\Delta G^{a,c}$ between disordered material (a) and well-ordered crystalline (c) solids.[59] There are related differences in ΔG for dissolution and consequently variations in particle solubility.[60] Therefore, amorphous and highly disordered materials have a higher solubility (K_{sp}) than crystalline materials.

Similar effects of structure on dissolution were reported for hematite nanoparticles of similar size and with different crystal structure and defect density.[61] Porter *et al.* also observed enhanced dissolution at grain boundaries of

hydroxyapatite in both *in-vivo* and *in-vitro* studies.[62] The pharmaceutical industry understands the impact of structure differences in solubility and uses it to enhance drug delivery. Hancock and Parks[60] note for even partially amorphous materials the solubility enhancement (theoretical or measured) is likely to influence *in-vitro* and *in-vivo* dissolution behavior. Much earlier work on the dissolution kinetics of calcite demonstrated that even the presence of significantly different concentrations of crystal dislocations could alter the dissolution rate of calcite by a factor of three.[63]

The amount of Ag dissolved in 24 h was nearly the same for $Ag^{Au}{}_{110}$NPs and $Ag^{pi}{}_{20}$NPs, and the apparent K_{sp} were relatively similar. We interpret this as an indication that the impact of the Au core on the particle structure diminished as particle size increases and note the Ag crystallites that made up the $Ag^{Au}{}_{110}$NPs were larger than the $Ag^{p}{}_{20}$NPs and the crystallite sizes of both were larger than Ag crystallites found in the $Ag^{Au}{}_{20}$NPs. It is well established that differences in size for nanoparticles can alter various types of particles properties,[64] but many size-dependent properties of nanoparticles do not change dramatically until the particle diameters less than 20–30 nm.[64–66] Therefore, significant differences in the solubility for 20 or 110 nm particles might not be expected based upon size alone, but might be understood based on differences in crystallinity.

Nanoparticles of various types are grown on seed crystals to help produce uniform size or obtain desired properties.[67–69] The current works shows that Ag grown on an Au seed crystal can impact particle structure, especially for shell thicknesses of size comparable or smaller than the core. However, other effects of a seed crystal or core on particle stability need to be considered. The contact potential difference between two metals can lead to galvanic corrosion, which would lead in this case to enhanced dissolution rates of Ag. Au–Ag alloys are a classic system for examining dealloying effects because only Ag dissolves.[70,71] However, galvanic corrosion occurs when both metals are exposed to the solution, which was not the case for the as-synthesized particles. In a study of dealloying of Au–Ag alloy nanoparticles, Star and Buttry[71] noted that an over potential was required to remove the Ag from these alloys and a subset of Ag atoms appeared to be protected by Au in the NP cores.

The presence of a gold core was used by others to help address questions related to the distribution of nanoparticles relative to dissolved Ag. Meng *et al.*[72] used gold-core Ag-shell nanorods to probe the biodistribution and toxic effect of silver NPs in mice. Using gold as a particle tracer made it possible to compare the particle distribution versus the Ag distribution, and they found limited distribution of particles relative to the much wider distribution of dissolved Ag. Such studies may help answer critical questions, but particles with the core–shell structure may in some circumstances behave differently than pure metal particles with different structure.

2. Effects of particle concentration

Understanding how particle concentrations impact particle aggregation, dissolution and other transformation provides critical information about the nature of cell exposure to the particles and solution Ag. The simple dissolution model described earlier fits the 24-h dissolution measurements reasonably well and provides a simple way to predict dissolution at different concentrations as well as a quantitative comparison of the behaviors of the different particles.

The observation from Table II that a single set of K_{sp} and k_+ parameters for each $Ag^{Au}{}_{20}$NPs, $Ag^{Au}{}_{110}$NPs, and $Ag^{pi}{}_{20}$NPs fit the dissolution data for particle loading from 9 to 50 μg/ml for the 24-h observation period indicates that the dissolution was relatively well behaved and could be usefully described by the simple model for the specific range of particle loadings and the 24-h period typical of many *in-vitro* experiments. The varying K_{sp} values highlight the differences in apparent solubility of the particles as discussed earlier. The $Ag^{Au}{}_{20}$NPs particles with the highest K_{sp} values were least stable and showed the highest dissolution in solution. The parameters in Table II can be used with Eq. (3) to estimate the integrated dose of dissolved Ag to which cells would be exposed during *in-vitro* studies. As suggested by the measured amounts dissolved Ag shown in Fig. 4, the amounts of dissolved Ag to which cells would be exposed would vary for the type of particles involved, but would be essentially independent of the particle loading for particle concentrations above 10 μg/ml.

C. Biological response

The cytotoxicity and oxidative stress measurements on macrophage cells indicate that structure/property differences between $Ag^{pn}{}_{20}$NPs and $Ag^{Au}{}_{20}$NPs can have biological consequences. These results provide information for more detailed mechanistic biological studies that are under way. The difference between cytotoxicity and oxidative stress may have implications related to the difference between chronic effects and acute toxicity as highlighted by Wang *et al.*[73] The results also shed some light on the relative importance of AgNPs versus dissolved Ag in the cell culture or exposure media.[74] Significant cytotoxic effects of exposure (Fig. 6) were not observed below particle concentrations of 25 μg/ml, although analysis of HMOX1 expression clearly indicated the induction of cellular oxidative stress at this dose level. Although there were differences in solution Ag between the two particle types for all particle loadings, within each particle type, there were virtually no differences in dissolved Ag as a function of particle exposure for particle loadings $\approx$10 μg/ml. Consequently, effects appearing at only higher doses suggest impacts of particle uptake and not differences in exposure to Ag dissolved from particles in the cell culture media. A potential explanation for these observations is that overt cytotoxicity of AgNPs occurs only after the level of intracellular Ag species reaches a critical level that overwhelms normal antioxidant defense capacity of cells. While extracellular dissolution may be insufficient to reach this critical point, there is no fundamental reason to expect that the differences in dissolution rates observed between different structural types of AgNPs do not also

operate intracellularly, thereby contributing to the differences in cytotoxicity observed among particle types at higher dose levels.

An impact of particles with a higher defect density is consistent with the observations of defect induced toxicity of George *et al.*[25] However, differences in solubility of the particles once within the cells might alter the amounts of internally dissolved Ag and internally dissolved Ag might be responsible for biological differences. Our observations specifically apply to RAW 264.7 macrophage cells exposed to AgNPs in the RPMI+10%FBS media as described in Scheme 1 and may not reflect observations of other cell types, cell culture media, or exposure conditions.

D. General discussion

1. Particle coatings and interactions with biological media

The interactions of nanoparticles with biological systems can be strongly influenced by the initial coatings on the particles being tested and the formation of protein layers or coronas that form in biological media.[24,75] A recent study found that citrate-AgNPs were more toxic than Polyvinylpyrrolidone (PVP)-AgNPs, despite having similar sizes and dissolution rates.[24] The authors proposed that Ag ions form complexes with PVP, which reduces their bioavailability and consequently cytotoxicity. Theodorou *et al.*[75] demonstrated that Ag ions may also undergo PVP-mediated reduction to form secondary AgNPs. These secondary particles, having a much smaller size could directly interfere with the function of cell membranes, allowing a larger number of AgNPs to penetrate inside cells.[34] They might also reach internal organelles more easily,[76] potentially inducing more pronounced toxic effects.

We have observed that dissolution of AgNPs is significantly accelerated when FBS is added to either DI water or the RPMI culture medium indicating that protein adsorption (corona formation) can assist dissolution. This raises the question of whether variations in the composition of protein coronas might partially explain either the observed differences in dissolution kinetics or biological responses. The presence of a protein corona can modulate cellular uptake and toxicity of AgNPs, though it is unclear specific corona proteins are critical for these effects.[77] While a direct comparison of the corona protein composition of AgNPs prepared with or without gold cores has not been done, a previous study reported the composition of proteins associated with the same $Ag^{Au}{}_{20}$NPs and $Ag^{Au}{}_{110}$NPs after incubation in culture medium containing 10% fetal bovine serum.[78] Mass spectrometry analyses identified common subsets of proteins that bound the AgNPs regardless of size or surface coating, including albumin, apolipoproteins, complement molecules, and other serum proteins. Although work by Podila *et al.*[79] had shown that surfactant free particles had a larger corona that particles surfactant stabilized, no clear relationships between surface coating (citrate or PVP) and the protein corona composition were found in this case (suggesting coatings such as citrate are readily displaced), size-dependent differences in protein adsorption suggest the enhanced curvature of 20 nm particles can result in preferential binding of some classes of proteins. Mass spectrometry analyses at PNNL (Kodali *et al.*, unpublished) confirmed these general observations. Future studies which determine whether specific subsets of these corona proteins serve as protein "sinks" for Ag ions would be informative to understand how the corona composition influences dissolution kinetics and cell responses.

Due to the complexity of the cell culture media (mixture of RPMI and FBS) and some of the complexation and corona effects noted above, we would not expect the simple dissolution model of Eq. (3) to adequately describe all of the processes that could take place. The simple dissolution model has at least two limitations observed in our studies. First, the parameters that fit the data above solution concentrations of 9 μg/ml significantly over-predicted the measured dissolution at lower particle concentrations. Second, additional data collected for longer than 24 h demonstrated that dissolution does not actually reach stable saturation values of dissolved Ag at 24 h as indicated by the fit to the simple model. The well-established tendency of silver ions to interact with organic molecules in aqueous media[80] likely contributes in different ways to both of these observed limitations.

It is relevant to recognize that the ICP-MS measurements used in this study measured all Ag that was in the supernatant, not just free Ag ions. Such data provided an appropriate indication of the amount of Ag dissolved from the particles, but included both ions in solution and Ag of any type that was not removed from the supernatant by the centrifuge process, including Ag entrained in proteins associated with FBS as well as any nonparticle (or very small particle) forms of Ag compounds that may have formed. The solubility product K_{sp} used in the simple model effectively assumes equilibrium between solid Ag and ions in solution, not taking into account any Ag tied to organic matter. Thus Ag ions may react (and possibly reduce) upon interaction with the serum proteins in solution creating a sink for Ag that is not represented in the current simple dissolution model. For data collection extended to periods as long as 72 h, no true saturation was observed. Although the simple model describes the data up to 24 h fit fair accuracy, it does not apply to longer times.

2. Daughter particle formation

The apparent lower effective solubility at lower particle loadings, producing lower K_{sp} values, seems to be counterintuitive. Using control studies, we verified that it is not the loss of Ag ions to the sample vessel wall or due to processing of the samples for ICP measurements. However, the small particles shown in Fig. 3 for dissolution with particle loadings of 1 μg/ml provided an important hint to what may be happening. The presence of daughter particles, or possibly particle fragments for the $Ag^{Au}{}_{20}$NPs, large enough to be observed by TEM was not apparent during TEM examination at higher particle loadings. These smaller particles were potentially large enough to be at least partially removed by

TABLE III. Range of particle sizes, dissolved Ag concentrations, and biological impacts reported in the literature.

Reference	Dissolution medium	Particle size (nm)	Dissolution time (h)	Nanoparticle concentration (μg/ml)	Dissolved Ag concentration (μg/ml)	Dissolved Ag (wt. %)	Conclusions on toxicity
31	Dulbecco's Modified Eagle Medium (DMEM)/ Fetal Calf Serum (FCS) 10%	20	24	5	0.85	17	Ag ion responsible for change in gene expression in a range of stress responses including oxidative stress, endoplasmic stress response, and apoptosis
		113	24	25	1.5	6	
6	RPMI 1640/FCS 10%	30	48	33	3.6	~11	Toxicity not due to Ag ions characterized by reduction in cell viability and increased lactate dehydrogenase release
32	Perchlorate buffer w/ dipalmitoylphosphatidylcholine pulmonary surfactant	14	72	25	>1.5	6	No toxicity studies performed
25	L-15 w/alignic acid	20	24	5	0.5	10	Ag ions induced oxidative stress effects. Nanoplates more toxic compared to spheres due to high surface reactivity
	Holtfereter w/alignic acid				0.07	1.4	
33	Hoagland	20	24	0.6	0.066	11	No toxicity studies performed
34	Bronchial Epithelial Cell Growth Medium	20	24	12.5	0.53	~4	Cellular toxicity and oxidative stress due to Ag ions
		110			0.31	~2.50	
35	KNO_3 w/bovine serum albumin	30	24	5	0.5	10	Hemolytic toxicity caused by Ag complexes like AgCl rather than free Ag ions
36	Not reported	~20	24	25	1.44	5.76	No hepatoxicity or immunotoxicity in rats by biochemical markers and antibody levels in blood, lymphocyte proliferation and cytokine release, and natural killer-cell activity
37	DMEM	10	24	10	2.36	23.6	Cell viability evaluated by lactate dehydrogenase assay and attributed to intracellular drug release

the centrifugation process.[81] As indicated by the discussion below, precipitation and growth of "larger" daughter particles appears to be favored at lower particles loadings.

It is well established that AgNPs can form in a variety of circumstances.[53,74,75,80,82] We note particularly that Akaighe *et al.*[80] observed formation of AgNPs by the reduction of Ag ions in the presence of humic acids; Goswami *et al.*[83] observed protein enabled nanoparticle growth; Panáček *et al.*[84] used a high molecular weight polymer to nucleate and control the size of Ag nanoparticles. They found the presence of poly(acrylic acid) (PAA), which forms a strong complex with Ag^+s, influenced both nucleation and growth of nanoparticles and that the size of the particles formed was larger when the concentration ratio of PAA/Ag was higher. An image of the particle formation and capture process shown in Fig. 6 in their paper[84] appears similar to our Figs. 3(b), 3(c), 3(e), and 3(f).

These reports suggest a possibility that AgNP formation could occur in our RPMI+FBS solution in the presence of Ag^+ and seed nanoparticles, and that the size of the particles formed might depend on the concentration of AgNPs present, the amount of dissolved Ag, and the protein concentration. To test the hypothesis that a small concentration of "parent" AgNPs in solution with Ag ions might lead to the formation of "daughter" smaller than the parent particles, but large enough to be removed by the centrifugation process used to separate nanoparticles from the supernatant, we measured Ag in the supernatant for a RPMI+FBS solution initially containing Ag ion concentration of 2.7 μg/ml (using $AgC_2H_3O_2$) and loadings of 0, 1, and 12.5 μg/ml of $Ag^{pn}{}_{20}$NPs. After 24 h, we were able to recover all or most of the initial concentration of supernatant Ag when only the Ag salt was present and when a concentration of 12.5 μg/ml of particles was present. However, for the solution containing 1 μg/ml of $Ag^{pn}{}_{20}$NPs, the amount of Ag measured in the supernatant was lowered by 50% (Fig. S11).[42] This measurement was consistent with the formation of nanoparticles large enough to be removed by centrifugation when low concentrations of AgNP particles—serving as seeds—were present in Ag^+ containing solution. The data also indicate that such particles were not present in significant quantities for initial particle loadings of 12.5 μg/ml or higher. It is also consistent with the TEM observations in Fig. 3. Thus the lower than expected amounts of Ag in the supernatant observed for particle loadings below 10 μg/ml in our dissolution data (lower apparent K_{sp} values relative to the values found for higher particle concentrations) appear to be due to the formation of daughter particles sufficiently large to be at least partially removed from the supernatant during the centrifugation process of Scheme 2.[81]

3. Range of Ag toxicity in the literature

The wide variety of responses to Ag reported in the literature as shown by examples in Table III, are likely due to variations in the biological systems being examined, the testing

media, the particle exposure, and/or the nature of the initial particles. Mechanistic understanding of important processes may require additional information that we are just beginning to understand and we may not yet have adequate data to parse some of these differences. In this study, the particles were the only variable showing the 20 nm particles made in different ways can have different physicochemical and biological impacts.

The ranges of variations of relevant parameters reported in literature regarding the dissolution and toxicology of AgNPs are shown in Table III. The solution concentration of Ag dissolved from the particles in 24 h ranged from 0.07 to 3.6 μg/ml (as a comparison, for the specific media, particles and protocols used in the studies reported in this paper and for initial particle loadings above 10 μg/ml, the dissolved Ag concentrations at 24 h ranged from 1 to 2.7 μg/ml). The biological impacts were not simply related to higher dissolved Ag concentration. For example, Bouwmeester *et al.*[31] reported dissolved Ag concentrations of 0.85 μg/ml for 20 nm particles for an initial and stress response. In contrast, Stoehr *et al.*[6] reported dissolved Ag concentrations of 3.6 μg/ml in RPMI 1640/FCS 10% for similar sized particles for an initial particle concentration of 33 μg/ml with no reported toxicity for spherical particles. Mechanistic understanding of important processes may require information that is not yet commonly available. For example, Gliga *et al.*[37] examined the effect of AgNPs versus ions released for cytotoxicity in human lung cells. Their data showed toxicity induced by AgNPs of size 10 nm while the free silver ions, as isolated from dissolution studies after 24 h, did not induce any toxicity. They concluded that toxicity was mainly responsible due to *intracellular* Ag release. In some cases, cells can protect themselves from Ag ions, but Ag particles may be able to penetrate the cell and then release ions, a Trojan horse mechanism.[74] Ag ion complexation may occur at multiple time scales, impacting dissolution, altering the nature of the Ag (ions, particles, or complexed in some way) interacting with cells, leading to formation of small particles and alternate pockets of Ag, thereby providing multiple sources of Ag to interact with a biological system.

The fate and solubility of particles in cells or biological systems may be highly dynamic. The traffic and fate of particles, their initial aggregation state, the cellular uptake processes involved, the nature of the media within the cell can all influence the nature of the particles and the solution Ag. The current studies were focused on understanding the bioavailability and stability of AgNPs as relevant for dosimetry modeling for *in-vitro* toxicity studies. Further work is needed to understand the transport and dissolution of particles into and with cells.

V. SUMMARY, CONCLUSION, AND PERSPECTIVES

The impact of AgNPs on biological systems depends on the initial nature of the particles, transformations they undergo in the media, the biological systems to which they are exposed, and the amount of dissolved Ag available for interaction. Results reported in this paper highlight and provide some quantitative information about the impact of particle structure on dissolution in one media and biological impact.

The detailed structure of nanoparticles depends on the synthesis process and particle history. As defects have been shown to impact particle toxicity in some circumstances, particles with widely different defect concentrations might reasonably be suspected to induce variations in biological response.

The 20 nm Ag particles formed around the Au core (Ag^{Au}_{20}NPs) were found to have high disorder (high number of grain boundaries) and an apparent higher effective solubility than the less disordered pure Ag particles, changing the amount of dissolved Ag present in biological media during times typical of *in-vitro* studies. In addition, the dissolution of the core–shell particles was less uniform in comparison to the pure particles, indicating that the structure of the particles can change significantly during dissolution. The 20 nm core–shell particles had a greater impact on RAW 264.7 macrophage cells. The nature of the dose response suggests that the differences in biological response are due to particle uptake and not dissolution in the cell culture media.

A simple dissolution model rationalized the impact of particle concentration on the rate of dissolution for particle concentrations between about 9 and 50 μg/ml for the media used in these studies. Although the simple model has several limitations, it can provide a helpful guide to understanding and predicting concentration effects for the time of many *in-vitro* experiments.

ACKNOWLEDGMENTS

The authors would like to thank Joel Pounds and Justin Teeguarden for many helpful discussions on toxicological implications of this work. Funding was provided by the National Institutes of Health, National Institute of Environmental Health Sciences under Grant No. U19 ES019544 (D.R.B. and B.D.T.) and U19ES19536 (A.P. and M.P.R.). Silver engineered nanomaterials and support was provided by the NIEHS Centers for Nanotechnology Health Implications Research (NCNHIR) Consortium. A.P. acknowledges a European Research Council starting grant for additional funding for S.C. (Project No. 257182). Portions of this work were performed using EMSL, a national scientific user facility sponsored by the U.S. Department of Energy, Biological and Environmental Research and located at PNNL.

[1]S. Arokiyaraj, M. V. Arasu, S. Vincent, N. U. Prakash, S. H. Choi, Y. K. Oh, K. C. Choi, and K. H. Kim, Int. J. Nanomed. **9**, 379 (2014).
[2]Q. H. Tran, V. Q. Nguyen, and A.-T. Le, Adv. Nat. Sci.: Nanosci. Nanotechnol. **4**, 033001 (2013).
[3]C. F. Dong, X. L. Zhang, and H. Cai, J. Alloys Compd. **583**, 267 (2014).
[4]K. L. N. Deepak, R. Kuladeep, K. S. Alee, and D. N. Rao, J. Nanosci. Nanotechnol. **12**, 920 (2012).
[5]J. Roh, J. Yi, and Y. Kim, Langmuir **26**, 11621 (2010).
[6]L. C. Stoehr, E. Gonzalez, A. Stampfl, E. Casals, A. Duschl, V. Puntes, and G. J. Oostingh, Part. Fibre Toxicol. **8**, 36 (2011).
[7]C. Levard, E. M. Hotze, G. V. Lowry, and G. E. Brown, Environ. Sci. Technol. **46**, 6900 (2012).

[8]J. Y. Liu and R. H. Hurt, Environ. Sci. Technol. **44**, 2169 (2010).
[9]Z. M. Xiu, Q. B. Zhang, H. L. Puppala, V. L. Colvin, and P. J. J. Alvarez, Nano Lett. **12**, 4271 (2012).
[10]M. Tejamaya, I. Romer, R. C. Merrifield, and J. R. Lead, Environ. Sci. Technol. **46**, 7011 (2012).
[11]J. Y. Liu, D. A. Sonshine, S. Shervani, and R. H. Hurt, ACS Nano **4**, 6903 (2010).
[12]J. Y. Liu, Z. Y. Wang, F. D. Liu, A. B. Kane, and R. H. Hurt, ACS Nano **6**, 9887 (2012).
[13]N. T. K. Thanh, N. Maclean, and S. Mahiddine, Chem. Rev. **114**, 7610 (2014).
[14]A. R. Tao, S. Habas, and P. Yang, Small **4**, 310 (2008).
[15]A. P. Z. Stevenson, D. B. Bea, S. Civit, S. A. Contera, A. I. Cerveto, and S. Trigueros, Nanoscale Res. Lett. **7**, 151 (2012).
[16]M. S. Shore, J. Wang, A. C. Johnston-Peck, A. L. Oldenburg, and J. B. Tracy, Small **7**, 230 (2011).
[17]A. Knauer, A. Eisenhardt, S. Krischok, and J. M. Koehler, Nanoscale **6**, 5230 (2014).
[18]M. Matzke, K. Jurkschat, and T. Backhaus, Ecotoxicology **23**, 818 (2014).
[19]E. Caballero-Díaz, C. Pfeiffer, L. Kastl, P. Rivera-Gil, B. Simonet, M. Valcárcel, J. Jiménez-Lamana, F. Laborda, and W. J. Parak, Part. Part. Syst. Charact. **30**, 1079 (2013).
[20]K. M. Tarquinio, N. K. Kothurkar, D. Y. Goswami, R. C. Sanders, A. L. Zaritsky, and A. M. LeVine, Int. J. Nanomed. **5**, 177 (2010).
[21]S. W. Kim, S. H. Nam, and Y. J. An, Ecotoxicol. Environ. Saf. **77**, 64 (2012).
[22]R. J. Griffitt, J. Luo, J. Gao, J. C. Bonzongo, and D. S. Barber, Environ. Toxicol. Chem. **27**, 1972 (2008).
[23]V. P. Hiriart-Baer, C. Fortin, D.-Y. Lee, and P. G. C. Campbell, Aquat. Toxicol. **78**, 136 (2006).
[24]A. A. Becaro, C. M. Jonsson, F. C. Puti, M. C. Siqueira, L. H. C. Mattoso, D. S. Correa, and M. D. Ferreira, Environ. Nanotechnol., Monit. Manage. **3**, 22 (2015).
[25]S. George *et al.*, ACS Nano **6**, 3745 (2012).
[26]U. Hansen and A. F. Thnemann, Langmuir **31**, 6842 (2015).
[27]A. M. Goodman, Y. Cao, C. Urban, O. Neumann, C. Ayala-Orozco, M. W. Knight, A. Joshi, P. Nordlander, and N. J. Halas, ACS Nano **8**, 3222 (2014).
[28]S. Kittler, C. Greulich, J. Diendorf, M. Koller, and M. Epple, Chem. Mater. **22**, 4548 (2010).
[29]J. Y. Liu, K. G. Pennell, and R. H. Hurt, Environ. Sci. Technol. **45**, 7345 (2011).
[30]C. Poland, M. Miller, R. Duffin, and F. Cassee, Part. Fibre Toxicol. **11**, 42 (2014).
[31]H. Bouwmeester *et al.*, ACS Nano **5**, 4091 (2011).
[32]B. F. Leo *et al.*, Environ. Sci. Technol. **47**, 11232 (2013).
[33]W. Zhang, Y. Yao, N. Sullivan, and Y. S. Chen, Environ. Sci. Technol. **45**, 4422 (2011).
[34]X. Wang *et al.*, Small **10**, 385 (2014).
[35]J. M. Zook, M. D. Halter, D. Cleveland, and S. E. Long, J. Nanopart. Res. **14**, 1165 (2012).
[36]M. van der Zande *et al.*, ACS Nano **6**, 7427 (2012).
[37]A. R. Gliga, S. Skoglund, I. O. Wallinder, B. Fadeel, and H. L. Karlsson, Part. Fibre Toxicol. **11**, 11 (2014).
[38]L. V. Stebounova, E. Guio, and V. H. Grassian, J. Nanopart. Res. **13**, 233 (2011).
[39]S. Chen *et al.*, Environ. Sci. Technol. **47**, 13813 (2013).
[40]S. Chen *et al.*, Nanoscale **5**, 9839 (2013).
[41]G. Sharma, V. Kodali, M. Gaffrey, W. Wang, K. R. Minard, N. J. Karin, J. G. Teeguarden, and B. D. Thrall, Nanotoxicology **8**, 663 (2014).
[42]See supplementary material at http://dx.doi.org/10.1116/1.4926547 for details of particle synthesis and history, DLS data and analysis, x-ray diffraction data, additional STEM and high resolution TEM images and the impact of particle loading on daughter particle nucleation.
[43]D. R. Baer *et al.*, J. Vac. Sci. Technol. A **31**, 050820 (2013).
[44]G. Maiorano, S. Sabella, B. Sorce, V. Brunetti, M. A. Malvindi, R. Cingolani, and P. P. Pompa, ACS Nano **4**, 7481 (2010).
[45]T. Miclaus, V. E. Bochenkov, R. Ogaki, K. A. Howard, and D. S. Sutherland, Nano Lett. **14**, 2086 (2014).
[46]Y. N. Xia, Y. J. Xiong, B. Lim, and S. E. Skrabalak, Angew. Chem. Int. Ed. **48**, 60 (2009).
[47]Y. Y. Ma, W. Y. Li, E. C. Cho, Z. Y. Li, T. K. Yu, J. Zeng, Z. X. Xie, and Y. N. Xia, ACS Nano **4**, 6725 (2010).
[48]P. Fenter and T. Gustaffson, Phys. Rev. B **43**, 12195 (1991).
[49]Lattice Constants of the Elements, Mathematica ElementData, see http://periodictable.com/Properties/A/LatticeConstants.html.
[50]M. Tsuji, N. Miyamae, S. Lim, K. Kimura, X. Zhang, S. Hikino, and M. Nishio, Cryst. Growth Des. **6**, 1801 (2006).
[51]L. Lartigue *et al.*, ACS Nano **7**, 3939 (2013).
[52]J. Liu, D. M. Aruguete, M. Murayama, and M. F. Hochella, Environ. Sci. Technol. **43**, 8178 (2009).
[53]R. D. Glover, J. M. Miller, and J. E. Hutchison, ACS Nano **5**, 8950 (2011).
[54]J. G. Teeguarden, P. M. Hinderliter, G. Orr, B. D. Thrall, and J. G. Pounds, Toxicol. Sci. **95**, 300 (2007).
[55]P. M. Dove and N. Han, "Kinetics of mineral dissolution and growth as reciprocal microscopic surface processes across chemical driving force," in *Perspectives on Inorganic, Organic and Biological Crystal Growth: From Fundamentals to Applications Directions*, edited by M. Skowronski, J. J. DeYores, and C. Wang, Am. Inst. Physics Conference Series 916 (2007), pp. 215–234.
[56]H. Zhang *et al.*, ACS Nano **6**, 4349 (2012).
[57]G. A. Orr, W. B. Chrisler, K. J. Cassens, R. Tan, B. J. Tarasevich, L. M. Markillie, R. C. Zangar, and B. D. Thrall, Nanotoxicology **5**, 296 (2011).
[58]T. Diedrich, A. Dybowska, J. Schott, E. Valsarni-Jones, and E. H. Oelkers, Environ. Sci. Technol. **46**, 4909 (2012).
[59]B. C. Hancock and G. Zografi, J. Pharm. Sci. **86**, 1 (1997).
[60]B. C. Hancock and M. Parks, Pharm. Res. **17**, 397 (2000).
[61]T. Echigo, D. M. Aruguete, M. Murayama, and M. F. Hochella, Geochim. Cosmochim. Acta **90**, 149 (2012).
[62]A. E. Porter, C. M. Botelho, M. A. Lopes, J. D. Santos, S. M. Best, and W. Bonfield, J. Biomed. Mater. Res., Part A **69A**, 670 (2004).
[63]J. Schott, S. Brantley, D. Crerar, C. Guy, M. Borcsik, and C. Willaime, Geochim. Cosmochim. Acta **53**, 373 (1989).
[64]M. Auffan, J. Rose, J.-Y. Bottero, G. V. Lowry, J.-P. Jolivet, and M. R. Wiesner, Nat. Nanotechnol. **4**, 634 (2009).
[65]M. F. Hochella, Earth Planet. Sci. Lett. **203**, 593 (2002).
[66]D. R. Baer *et al.*, Surf. Interface Anal. **40**, 529 (2008).
[67]C. C. Li, L. Sun, Y. Q. Sun, and T. Teranishi, Chem. Mater. **25**, 2580 (2013).
[68]Y. C. Tsao, S. Rej, C. Y. Chiu, and M. H. Huang, J. Am. Chem. Soc. **136**, 396 (2014).
[69]N. R. Jana, L. Gearheart, and C. J. Murphy, Langmuir **17**, 6782 (2001).
[70]J. Erlebacher and K. Sieradzki, Scr. Mater. **49**, 991 (2003).
[71]C. A. Starr and D. A. Buttry, ECS Trans. **58**, 19 (2014).
[72]J. Meng, Y. L. Ji, J. Liu, X. L. Cheng, H. Guo, W. Q. Zhang, X. C. Wu, and H. Y. Xu, Nanotoxicology **8**, 686 (2014).
[73]Z. Wang, T. Xia, and S. Liu, Nanoscale **7**, 7470 (2015).
[74]B. Reidy, A. Haase, A. Luch, K. A. Dawson, and I. Lynch, Materials **6**, 2295 (2013).
[75]I. Theodorou *et al.*, Environ. Sci. Technol. **49**, 8048–8056 (2015).
[76]C. Carlson, S. M. Hussain, A. M. Schrand, L. K. Braydich-Stolle, K. L. Hess, R. L. Jones, and J. J. Schlager, J. Phys. Chem. B **112**, 13608 (2008).
[77]J. H. Shannahan, R. Podila, A. A. Aldossari, H. Emerson, B. A. Powell, P. C. Ke, A. M. Rao, and J. M. Brown, Toxicol. Sci. **143**, 136 (2015).
[78]J. H. Shannahan, X. Lai, P. C. Ke, R. Podila, J. M. Brown, and F. A. Witzmann, Plos One **8**, e74001 (2013).
[79]R. Podila, R. Chen, P. C. Ke, J. M. Brown, and A. M. Rao, Appl. Phys. Lett. **101**, 263701 (2012).
[80]N. Akaighe, R. I. MacCuspie, D. A. Navarro, D. S. Aga, S. Banerjee, M. Sohn, and V. K. Sharma, Environ. Sci. Technol. **45**, 3895 (2011).
[81]*Gold Nanoparticle Storage & Handling*, edited by Cytodiagnostics (Cytodiagnostics, Burlington, ON), Technical Note: 101, see http://www.cytodiagnostics.com/technical_notes.php.
[82]Y. G. Yin, J. F. Liu, and G. B. Jiang, ACS Nano **6**, 7910 (2012).
[83]N. Goswami, R. Saha, and S. Pal, J. Nanopart. Res. **13**, 5485 (2011).
[84]A. Panáček, R. Prucek, J. Hrbáč, T. J. Nevečná, J. Šteffková, R. Zbořil, and L. Kvítek, Chem. Mater. **26**, 1332 (2014).